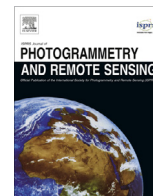




Contents lists available at ScienceDirect

ISPRS Journal of Photogrammetry and Remote Sensing

journal homepage: www.elsevier.com/locate/isprsjprs

Spectral analysis of amazon canopy phenology during the dry season using a tower hyperspectral camera and modis observations



Yhasmin Mendes de Moura ^{a,*}, Lênio Soares Galvão ^a, Thomas Hilker ^{b,1}, Jin Wu ^{c,d}, Scott Saleska ^c, Cibele Hummel do Amaral ^e, Bruce Walker Nelson ^f, Aline Pontes Lopes ^a, Kenia K. Wiedeman ^{c,g}, Neill Prohaska ^c, Raimundo Cosme de Oliveira ^h, Carolyn Bueno Machado ^a, Luiz E.O.C. Aragão ^{a,i}

^a Instituto Nacional de Pesquisas Espaciais (INPE), Avenida dos Astronautas, 1758, São José dos Campos, SP CEP 12245-970, Brazil

^b University of Southampton, Department of Geography and Environment, Southampton SO17 1BJ, United Kingdom

^c University of Arizona, Department of Ecology and Evolutionary Biology, Tucson, AZ 85721, United States

^d Environmental and Climate Science Department, Brookhaven National Laboratory, Upton, NY, 11973, United States

^e Universidade Federal de Viçosa, MG 36570-900, Brazil

^f Instituto Nacional de Pesquisa da Amazônia (INPA), Departamento de Dinâmica Ambiental, Av. André Araújo, 2936, Manaus, AM 69067-375, Brazil

^g John A. Paulson School of Engineering and Applied Sciences, Harvard University, Cambridge, MA 02138, United States

^h Empresa Brasileira de Pesquisa Agropecuária (EMBRAPA), Centro de Pesquisa Agroflorestal da Amazônia Oriental, 66095100 Belém, PA, Brazil

ⁱ College of Life and Environmental Sciences, University of Exeter, EX4 4RJ, United Kingdom

ARTICLE INFO

Article history:

Received 4 April 2017

Received in revised form 8 June 2017

Accepted 15 July 2017

Keywords:

Phenology

Hyperspectral remote sensing

Tropical species

Leaf flush

Amazon

Seasonality

Dry season

ABSTRACT

The association between spectral reflectance and canopy processes remains challenging for quantifying large-scale canopy phenological cycles in tropical forests. In this study, we used a tower-mounted hyperspectral camera in an eastern Amazon forest to assess how canopy spectral signals of three species are linked with phenological processes in the 2012 dry season. We explored different approaches to disentangle the spectral components of canopy phenology processes and analyze their variations over time using 17 images acquired by the camera. The methods included linear spectral mixture analysis (SMA); principal component analysis (PCA); continuum removal (CR); and first-order derivative analysis. In addition, three vegetation indices potentially sensitive to leaf flushing, leaf loss and leaf area index (LAI) were calculated: the Enhanced Vegetation Index (EVI), Normalized Difference Vegetation Index (NDVI) and the entitled Green-Red Normalized Difference (GRND) index. We inspected also the consistency of the camera observations using Moderate Resolution Imaging Spectroradiometer (MODIS) and available phenological data on new leaf production and LAI of young, mature and old leaves simulated by a leaf demography-ontogeny model. The results showed a diversity of phenological responses during the 2012 dry season with related changes in canopy structure and greenness values. Because of the differences in timing and intensity of leaf flushing and leaf shedding, *Erismia uncinatum*, *Manilkara huberi* and *Chamaecrista xinguensis* presented different green vegetation (GV) and non-photosynthetic vegetation (NPV) SMA fractions; distinct PCA scores; changes in depth, width and area of the 681-nm chlorophyll absorption band; and variations over time in the EVI, GRND and NDVI. At the end of dry season, GV increased for *Erismia uncinatum*, while NPV increased for *Chamaecrista xinguensis*. For *Manilkara huberi*, the NPV first increased in the beginning of August and then decreased toward September with new foliage. Variations in red-edge position were not statistically significant between the species and across dates at the 95% confidence level. The camera data were affected by view-illumination effects, which reduced the SMA shade fraction over time. When MODIS data were corrected for these effects using the Multi-Angle Implementation of Atmospheric Correction Algorithm (MAIAC), we observed an EVI increase toward September that closely tracked the modeled LAI of mature leaves (3–5 months). Compared to the EVI, the GRND was a better indicator of leaf flushing because the modeled production of new leaves peaked in August and then declined in September following the GRND closely. While the EVI was more related to changes in mature leaf area, the GRND was more associated with new leaf flushing.

© 2017 International Society for Photogrammetry and Remote Sensing, Inc. (ISPRS). Published by Elsevier B.V. All rights reserved.

* Corresponding author.

E-mail address: yhas.mendes@gmail.com (Y.M. de Moura).

¹ In Memoriam.

1. Introduction

Terrestrial ecosystems regulate carbon–climate feedbacks by controlling fluxes of mass and energy between the biosphere and the atmosphere (Bonan et al., 2003). In turn, changes of the biosphere's carbon balance (i.e. uptake or losses) affect the climate system (Friedlingstein et al., 2006; Frank et al., 2015). However, detailed knowledge of the processes and mechanisms of the carbon cycle is still lacking. A better understanding of these feedbacks is urgently needed to reduce climate model uncertainties and to allow more accurate predictions of vegetation changes under future climate scenarios. This is particularly important in the tropics, where high plant productivity sustains one of the largest remaining terrestrial carbon pools on the planet (Hilker et al., 2014; Wu et al., 2016a). The ongoing exposure of tropical ecosystems to anthropogenic pressures and climatic changes have led to substantial concerns about the future of tropical forests as a component of the global climate system (Cox et al., 2004; Malhi et al., 2008). While field experiments, networks of flux-towers and remote sensing based studies have improved our understanding on the sensitivity of forests to climate in temperate regions (e.g., D'Odorico et al., 2015; Gamon et al., 2006; Hilker et al., 2010; Richardson et al., 2007, 2012; Yang et al., 2014), this issue is far less understood in the tropics.

Quantifying shifts in phenological cycles, which influences the timing of plant maximum photosynthetic activity, is critical for describing tropical ecosystem metabolism and environmental controls (Cleland et al., 2007; Richardson et al., 2012; Wu et al., 2016a). However, phenological observations in tropical regions have proven challenging (Samanta et al., 2010) and so far have been unable to produce unequivocal evidence for the constraints of vegetation growth in the tropics (Huete et al., 2006; Lee et al., 2013; Borchert et al., 2015; Guan et al., 2015; Bi et al., 2015). Despite the uncertainty associated with the mean seasonality of vegetative growth derived from satellite remote sensing, it is even more controversial when using these remote sensing observations to explore tropical forest response to inter-annual droughts (Myneni et al., 2007; Morton et al., 2014; Saleska et al., 2016). An increase in greenness (higher Enhanced Vegetation Index - EVI) for the 2005 drought was reported by Saleska et al. (2007), whereas a widespread decline in photosynthetic activity (lower EVI) for the 2010 drought was observed by Xu et al. (2011). While remote sensing approaches have shown conflicting results, field-based studies indicate that moisture stress in tropical forests due to extreme events of droughts reduces aboveground biomass growth and increases tree mortality, altering carbon stocks and biodiversity (Phillips et al., 2009).

To date, tropical leaf phenology remains one of the most challenging components to parameterize in ecosystem models (Arora and Boer, 2005). Part of the observational uncertainties has been linked to poor quality remote sensing data because of high atmospheric aerosol loadings and deficiencies in cloud detection and screening (Samanta et al., 2010; Hilker et al., 2014). Progress has been made with the development of more robust atmospheric correction methods (e.g. Multi-Angle Implementation of Atmospheric Correction - MAIAC) (Lyapustin et al., 2011), or the use of higher spatial resolution imagery (Zelazowski et al., 2011). However, a scale mismatch remains between moderate to coarse spatial resolution satellite imagery on one hand, and a sparse network of field observations on the other.

One possible approach to address this mismatch and to help further our understanding of tropical phenology is to use observations from tower-based cameras to consistently link optical signals with biophysical processes. Near surface, camera-based phenology can help bridging the spatial mismatch existing between field and

satellite data by using optical principles similar to those used by spaceborne optical sensors, but still allowing interpretations similar to those made at the plot level.

In temperate regions, tower-based optical remote sensing has been used to establish frequent observations of plant phenology (Richardson et al., 2007), to link them to biophysical processes of photosynthesis (Hilker et al., 2010), and to scale-up field observations (D'Odorico et al., 2015). Perhaps most prominently, the phenocam network (Richardson et al., 2007) provides a continental-scale phenological observatory, spanning a range of biogeoclimatic zones in North America. Other networks (Gamon et al., 2006) and individual studies have been undertaken to connect optical measurements and flux tower observations of CO₂ exchange and ecosystem productivity using multi-angular (Hilker et al., 2010; Tortini et al., 2015) and mono-angle spectroscopy (Garbulsky et al., 2008; Garrity et al., 2010).

More recently, tower-based observations of plant phenology have also been established for tropical vegetation using near infrared (NIR)-red-green cameras (Wu et al., 2016a) and simple RGB cameras (Lopes et al., 2016). Increases in dry season “Amazon greening” were linked to synchronous leaf flushing during the dry season in central Amazonia, in response to an increase in available PAR, consistent with previous satellite studies (Huete et al., 2006; Anderson et al., 2011; Guan et al., 2015) and field investigations (Restrepo-Coupe et al., 2013). Increases in vegetation greenness were preceded by abrupt, brief “browning” because of the increased leaf abscission (Lopes et al., 2016). While tower-based observations have improved our understanding of plant phenology in the tropics, a comprehension of its effect on the optical signal observed by hyperspectral instruments in different regions of the electromagnetic spectrum is currently lacking, as is an understanding of the spatial heterogeneity of the observed signal. Such understanding will be critical in order to assess tropical seasonality at broader scales using future orbital hyperspectral missions such as the Environmental Mapping and Analysis (EnMAP), planned for 2019 (Ganter et al., 2015), and the Hyperspectral Infrared Imager (HyspIRI), planned for the near future (Hochberg et al., 2015), both with 30 m spatial resolution.

The objective of this paper was to analyze spectral components of canopy phenology using a tower-mounted hyperspectral camera in an eastern Amazon forest to assess dry season differences existing between individual species. Our analysis was based on hyperspectral data acquired during the 2012 dry season at the k67 flux-tower field station in the Tapajós National Forest (TNF), in Brazil. As far as we know, this is the first hyperspectral remote sensing study using a tower-mounted camera to observe canopy phenology in the Amazon.

Our study was designed to address four research questions: (1) How do individual components (leaves, branches and shade) of tropical species canopy vary throughout the dry season? (2) What are the most important spectral components responsible for the data variance in the hyperspectral signal to describe phenological patterns across species? (3) Are there dry season variations in spectral attributes and metrics between the species? (4) Are the phenological patterns observed from the tower-based hyperspectral data perceptible when evaluating a landscape level data (MODIS observations)?

2. Data acquisition and processing

2.1. Hyperspectral data acquisition

The study area in Brazil is the TNF, located in the eastern Amazon, near Santarém town, in the state of Pará, which is mainly composed of dense ombrophilous forest (Fig. 1). The climate in the

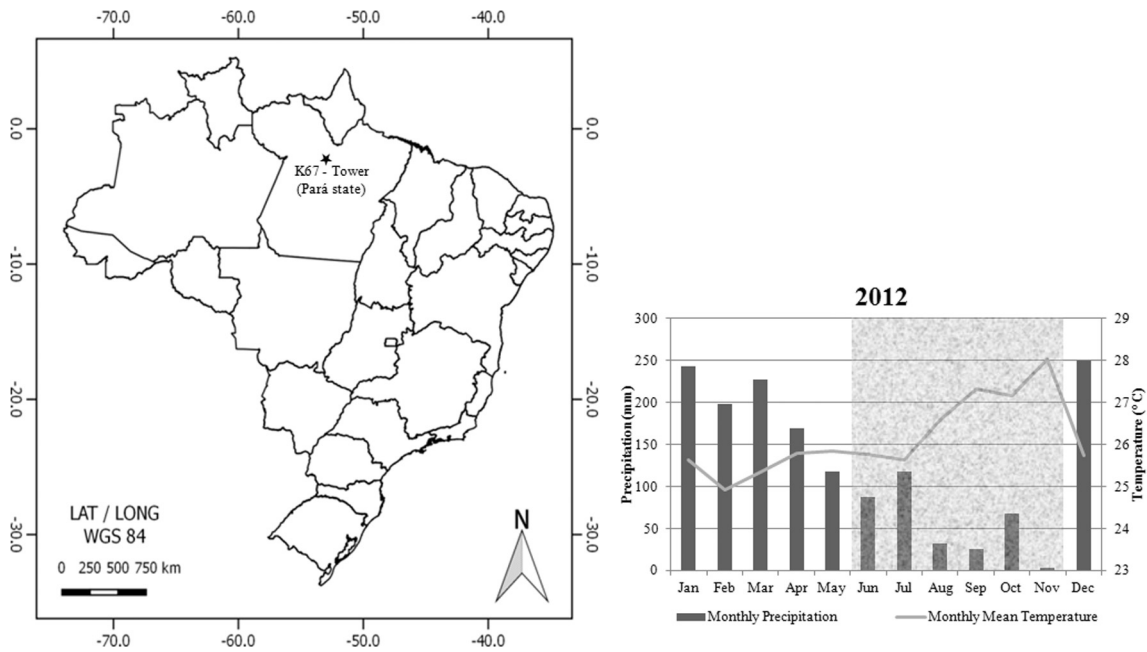


Fig. 1. At the left side, we show the location of the k67-tower (star) in the Tapajós National Forest, eastern Amazon, in the state of Pará, Brazil. At the right side, we plot monthly precipitation and mean temperature for 2012, obtained from a meteorological station (Belterra municipality). The shaded portion of the figure indicates the dry season.

Köppen classification is tropical AmW (monsoon type with short dry season) with a mean precipitation of $1700 \text{ mm year}^{-1}$ and an average dry season length of five months between July and November (Aragão et al., 2008). The mean annual temperature is $26 \text{ }^{\circ}\text{C}$. In the 2012 dry season, the monthly precipitation decreased from 120 mm in July to 5 mm in November, while the mean temperature increased from $25.6 \text{ }^{\circ}\text{C}$ to $28.6 \text{ }^{\circ}\text{C}$ (Fig. 1). The local topography is relatively flat with an altitude below 200 m . *Latossolo Amarelo distrófico* (Xanthic Acrustox in the USA Soil Taxonomy) is the predominant soil type in the study area.

We used data acquired by a hyperspectral Surface Optics 710 Camera (SOC; Surface Optics Corporation, San Diego, CA) in the dry season of 2012 between July 29 and September 25. The camera was mounted at a height of 61 m on the Tapajós k67 eddy covariance tower (2.85°S , 54.97°W). The hyperspectral sensor acquired images in 128 narrow bands (bandwidth of 5 nm) positioned between 388 nm and 1051 nm . To ensure confidence in the data analysis and avoid noisy data, we considered only the $437\text{--}898 \text{ nm}$ spectral range. As a result, the leaf/canopy water feature centred at 980 nm was not evaluated here. Seventeen images were carefully selected and screened for clear sky conditions and data quality in the $437\text{--}898 \text{ nm}$ range. A White Teflon panel, permanently installed within the field of view of the camera, was used as reference for calibrating the data. Images were acquired at off-nadir viewing (45°) in the backscattering direction and around solar noon ($11:30 \text{ a.m.}$ local time) to reduce shading effects within- and among the canopies in each date.

2.2. Analysis of hyperspectral images

We focused our analysis of the 17 hyperspectral images on three species (*Erismia uncinatum* Warm., *Manilkara huberi* (Ducke) A. Chev. and *Chamaecrista xinguensis* (Ducke) H.S.Irwin & Barneby), which are common at the k67 site. *Erismia uncinatum* and *Manilkara huberi* alone accounts for 16% of basal area of the vegetative community of the site. *Erismia uncinatum* Warm. generally has large trees with diameter at breast height (DBH) up to 148 cm and

maximum canopy height (MCH = 40 m) greater than that observed for *Manilkara huberi* (maximum DBH = 91 cm ; MCH = 37 m), as reported by Wu et al. (2016a). *Chamaecrista xinguensis* presented canopy heights between 15 and 30 m , but was also sunlit, as the Tapajós forest has a very irregular canopy.

Crowns representing different trees of these species were delineated manually over the hyperspectral images to reduce shade by neighbor or emergent trees. To represent the vegetation response over time using different hyperspectral metrics, we selected randomly 150 pixels per species and date, which were kept fixed in position over the sunlit crowns, whenever possible. We applied *t*-tests to verify whether the differences in metric means between the beginning and end of the time series were statistically significant at 95% confidence level.

Several techniques and procedures were used for processing the hyperspectral data. They included the linear spectral mixture analysis (SMA), principal component analysis (PCA), continuum removal analysis (CR), derivative analysis (DA) and vegetation indices (VI), as described below.

2.2.1. Spectral mixture analysis (SMA)

How do individual components (leaves, branches and shade) of tropical species canopies vary throughout the dry season? In order to answer this question and analyze phenological variations over time, we applied SMA to each of the 17 hyperspectral images. SMA assumes that the reflectance of each pixel is a linear combination of the endmember reflectance values (van der Meer, 2004). Therefore, the first step in SMA is to define image-derived endmembers, which was performed here using the July dataset. In the absence of pixels representing bare soil in the images, we selected a three-endmember model composed of green vegetation (GV), non-photosynthetic vegetation (NPV) and shade. To select the first two endmembers, we first applied the minimum noise fraction (MNF) algorithm to separate the signal-dominated components from the noise-dominated images (Green et al., 1988). The first MNF images having large eigenvalues and good image quality were then used as input data for the pixel purity index (PPI)

technique to find pure endmembers. We set up the number of interactions to 5000 and the threshold to 2.5 of the MNF normalized noise. Candidate endmembers for GV and NPV detected automatically by the PPI were projected into an n -dimensional scatterplot for final endmember selection looking at the corner of the data clouds (Galvão et al., 2011). From the use of the PPI technique applied to the first 12 MNF images having eigenvalues greater than two and cumulative data variance greater than 90%, we selected a GV spectrum from *Erisma uncinatum* and a NPV spectrum from *Chamaecrista xinguensis* as endmembers to compose a three-endmember model with shade. Following the procedure described by Roberts et al. (1993), the shade endmember used in this study had constant low reflectance to represent pure shade in all bands, spectrally flat in the 437–898 nm range.

The fixed set of three endmembers was then used in the SMA to generate fraction images. The singular value decomposition approach was used as a solution for data inversion into the fraction images of each date. Endmember-fraction values were then plotted for each species over time to inspect canopy phenology during the dry season.

2.2.2. Principal component analysis (PCA)

What are the most important spectral intervals responsible for the data variance in the hyperspectral signal to describe phenological patterns across species? PCA is a technique to handle highly correlated reflectance values across bands, to reduce data dimensionality and to detect the most important spectral bands, responsible for most of the data variance in the original variables (Moreira and Galvão, 2010). Here, we applied PCA to a set of 7650 pixels (150 pixels, 3 species and 17 dates) to identify patterns of canopy phenology, using the reflectance of the 89 SOC camera bands positioned between 437 and 898 nm as input variables. We applied PCA to the set of 150 selected sunlit pixels (based on the crowns of each specie) instead of the entire image to reduce sun/canopy illumination effects on the interpretation of results and to give equal weight to each species, thus enhancing their phenological differences.

Extraction of the components was based on the correlation matrix and on eigenvalues responsible for more than 90% of the cumulative data variance. In the identification of patterns of canopy phenology, two principal components with eigenvalues greater than two were retained. The contribution of each band to explain each component was determined from the analysis of the component matrix loadings. Sampling adequacy and data suitability for reduction were examined using the Kaiser-Meyer-Olkin (KMO) measure and Bartlett's test of sphericity, respectively (Cerny and Kaiser, 1977). We obtained and plotted the scores for the first components without rotation and analyzed the spectral similarity between the three species. Because PCA is very sensitive to outliers, we used scores greater than four standard deviations away from the mean to detect and remove them from the analysis before running again the algorithm.

2.2.3. Continuum removal, derivative analysis and vegetation indices

Are there dry season variations in spectral attributes and metrics between the species? To answer this question, we calculated on a per pixel basis the depth, width, area and asymmetry of the chlorophyll absorption band centred at 680 nm for the 17 images. We used the Processing Routines in IDL for Spectroscopic Measurements (PRISM) software (Kokaly and Skidmore, 2015). The PRISM is based on the well-established continuum removal approach, which isolates absorption bands from the spectra to allow quantification of their parameters (Clark and Roush, 1984). We fixed the wavelengths at 560 nm and 760 nm (shoulders of the absorption band) to remove the continuum. Absorption band parameters were

then plotted as a function of the species and of the date of image acquisition.

In addition, derivative analysis detected the red-edge spectral position, which is the wavelength of maximum first derivative of the reflectance spectrum between 690 nm and 750 nm. The red-edge position is potentially sensitive to changes in chlorophyll concentration (Cho and Skidmore, 2006; Clevers and Gitelson, 2013). In our study, the first-order transformation was preceded by the Savitzky-Golay smoothing method for removing the background noise using a window size of three bands. Variations in red-edge position over time were analyzed per species.

Finally, we calculated the Normalized Difference Vegetation Index (NDVI) and the EVI to study their sensitivity to some phenological events in the study area. For this purpose, we used the narrow bands of the hyperspectral camera positioned at 472 nm (blue), 661 nm (red) and 861 nm (NIR). Both indices are the main components of the Moderate Resolution Imaging Spectroradiometer (MODIS) vegetation index products (Huete et al., 2002). They have been widely used in studies of the Amazonian tropical forests (e.g., Huete et al., 2006; Saleska et al., 2007; Galvão et al., 2011; Moura et al., 2012). Equations and parameters were the same as the MODIS products.

After the analysis of leaf flushing events from neighboring branches of a given species under the same illumination conditions, we additionally tested the potential of the normalized difference between the green (563 nm) and red (661 nm) reflectance (ρ) to detect leaf flushing. Henceforth, to facilitate reading, this VI is entitled the Green-Red Normalized Difference (GRND) (Eq. (1)):

$$\text{GRND} = (\rho_{563\text{nm}} - \rho_{661\text{nm}}) / (\rho_{563\text{nm}} + \rho_{661\text{nm}}) \quad (1)$$

The GRND is conceptually similar to the Green Chromatic Coordinate, a greenness index defined as the fractional contribution of the green spectral response to the summed response of the blue, green and red channels in a RGB camera (Woebbecke et al., 1995). In our study, we avoid using the blue band in the GRND equation to reduce uncertainties associated with atmospheric scattering when calculating this index from MODIS data.

2.3. From tower hyperspectral measurements to MODIS (MAIAC) observations

Are the phenological patterns observed from the tower-based hyperspectral data perceptible when evaluating a landscape level data (1-km MODIS observations)? Because the hyperspectral camera sensed a small footprint at the k67 Tapajós tower (300 m), we compared our tower-based results with biweekly MODIS data processed by the MAIAC (Lyapustin et al., 2011). MAIAC applies rigorous cloud screening and atmospheric correction to obtain surface reflectance without typical empirical assumptions. MODIS (MAIAC) data were corrected for Bidirectional Reflectance Distribution Function (BRDF) effects, normalized to nadir viewing and to a fixed solar zenith angle (SZA) of 45°. The BRDF correction reduces the error and bias associated with view-illumination geometry that affects differently the VIs. To compare the results, we calculated the NDVI (MODIS bands 1 and 2), EVI (bands 1, 2 and 3) and the GRND (bands 1 and 4) for a 3 × 3 km footprint at the tower site and plotted the long-term mean (2000–2014) for the dry season to reduce noise in the time series.

Due to sample size limitations of the camera data, MODIS observations were compared with a landscape model of monthly LAI partitioned into three leaf age classes. This approach was used to inspect the consistency of the tower and MODIS results with ground-based observations of canopy phenology. We used available data on new leaf production and leaf area index (LAI) of young (1–2 months), mature (3–5 months) and old (≥ 6 months) leaves simulated from a leaf demography-ontology model (Wu et al.,

2016a). The simulation was supported by LAI (LAI-2000) and litter-fall (traps) measurements (2000–2005). We plotted the simulated new leaf production (Wu et al., 2016a) and LAI against the MODIS (MAIAC) VIs.

3. Results

3.1. Spectral components of canopy phenology from SMA

Dry season differences in canopy phenology between the species were clearly visible in true color composites of the hyperspectral camera using bands positioned at 661 nm, 563 nm and 487 nm in red, green and blue, respectively (Fig. 2). For instance, *Erismia uncinatum* (green line in Fig. 2) became brighter from July 29 (DOY 211) to September 25 (DOY 269), while *Chamaecrista xinguensis* (red line) lost leaves toward the end of the dry season.

Endmember spectra for SMA are shown in Fig. 3. Distinct patterns of canopy phenology per species were observed in SMA color composites using GV, NPV and shade fractions in green, red and blue colors, respectively (Fig. 4). *Erismia uncinatum* had increasing GV fractions toward the end of dry season, as indicated by brighter green colors observed from DOY 211 to 269. In contrast, *Chamaecrista xinguensis* had increasing NPV fractions with deciduousness, as shown by the predominance of magenta shades in the images of September (DOY 247–269). The behavior of *Manilkara huberi* was different from the other two species (Fig. 4). The NPV first increased in the beginning of August (magenta shades in the DOY 218 and 227 images) and then decreased in the subsequent dates (green tones) with new foliage.

Results of Fig. 4 were confirmed when we plotted the average GV (Fig. 5a) and NPV (Fig. 5b) fractions calculated from 150 pixels randomly chosen per species and date. The contrasting phenological behavior between the evergreen *Erismia uncinatum* and the deciduous *Chamaecrista xinguensis* was evident in the SMA fractions, because these species presented the largest mean GV (42–50%) and NPV (13–25%) values, respectively. When compared to *Erismia uncinatum*, the evergreen *Manilkara huberi* had lower mean GV fraction and higher mean NPV fraction, especially in the beginning of August.

For the entire hyperspectral camera scene, the number of pixels with shade fraction greater than 60% decreased from July to September, revealing the influence of view-illumination effects during the dry season (Fig. 6). The 17 images were acquired around the noon (11:30 a.m.) but the solar zenith angle (SZA) decreased 13° from July 29 (SZA = 28°) to September 25 (SZA = 15°) (Fig. 7). In addition, the solar azimuth angle (SAA) increased toward the end of the dry season from 40° to 85°. As a result, the relative azimuth angle (RAA) between the camera and the sun also decreased over time with the sensor becoming more aligned to the direction of illumination (principal plane) toward September. Therefore, along with leaves density and distribution, view-illumination effects contributed for the reduced amounts of shadows and the increased amounts of leaf/canopy scattering sensed by the tower-mounted camera at the end of September. For the two non-deciduous species, GV increased gradually over the period mainly due to decreasing shade and not at the expense of NPV, since NPV did not decrease for these two species in the lower graph of Fig. 5.

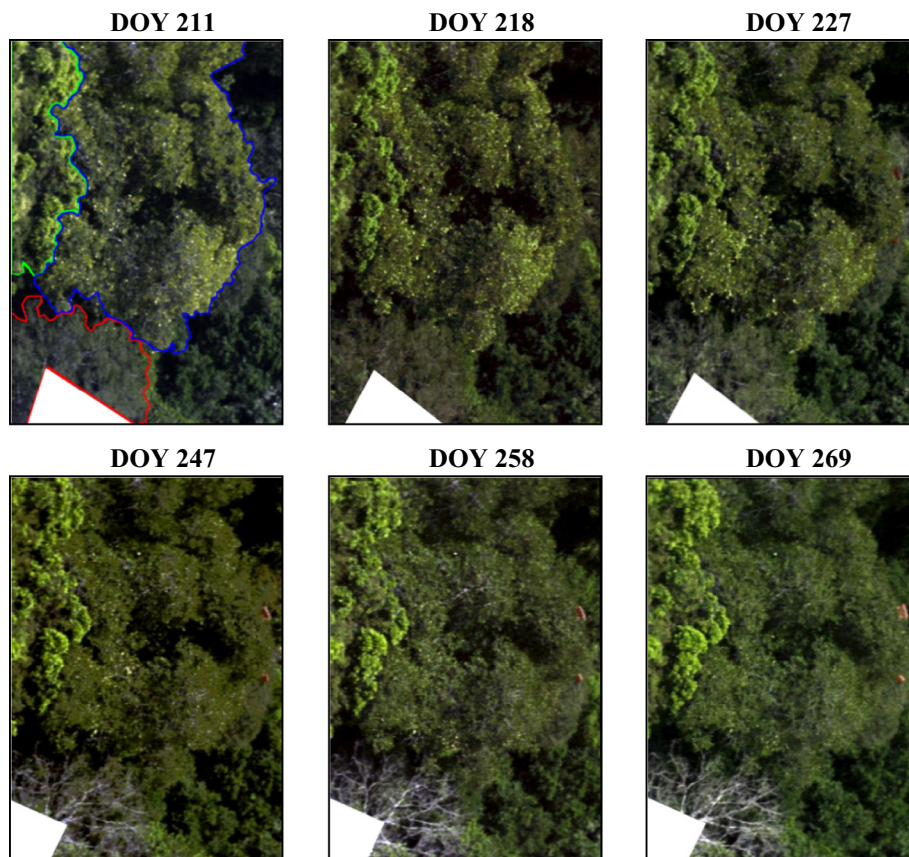


Fig. 2. Time series for six of the 17 true color composites of canopy phenology observed from the hyperspectral camera mounted at the k67 tower in Tapajós. The green, blue and red lines for the first date delineate the three species: *Erismia uncinatum*, *Manilkara huberi* and *Chamaecrista xinguensis*, respectively. (For interpretation of the references to color in this figure legend, the reader is referred to the web version of this article.)

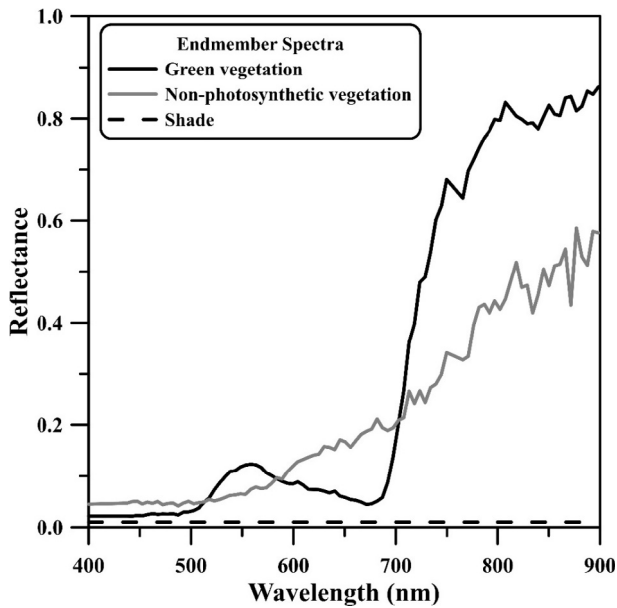


Fig. 3. Green and non-photosynthetic endmember spectra for spectral mixture analysis (SMA) selected from the sequential use of the minimum noise fraction (MNF) and pixel purity index (PPI) techniques. Shade is represented by a synthetic spectrum of flat low reflectance across all wavebands.

3.2. Canopy phenology detected by PCA

Using the Bartlett Test of sphericity, we rejected the null hypothesis that the correlation matrix was an identity matrix (p -value < 0.001), indicating that it was highly unlikely to have obtained the correlation matrix from a population with zero correlation. The Kaiser-Meyer-Olkin (KMO) measure was closer to one (0.99), thus indicating sampling adequacy for PCA. The first two principal components were responsible for 90.1% of the cumulative variance of the data. PC1 accounted for 61.5% of variance, while PC2 captured 29.6% of variance. The analysis of the component matrix loadings, which are the correlations between the band reflectance and the component, showed that most of the SOC camera bands had large loadings on PC1, especially between 500 and 650 nm and between 700 and 898 nm (Fig. 8). Therefore, PC1 reflected brightness variations between the pixels. PC1 increased with increasing reflectance of these bands. By contrast, PC2 showed large positive loadings in the blue (450–490 nm) and in the chlorophyll red absorption region (650–680 nm), and negative loadings in the NIR region between 750 and 898 nm. PC2 increased with increasing blue and red reflectance and with decreasing NIR reflectance. Thus, PC2 was sensitive to variations in NPV across pixels. The three species were separated from each other based on their average reflectance (PC1) and average NPV content (PC2) over time.

Differences in canopy phenology between the three species are illustrated by projecting the first two PC scores for each of the 7650 pixels extracted from the 17 dates of image acquisition (Fig. 9). The species clustered differently in the PCA space. Confirming the

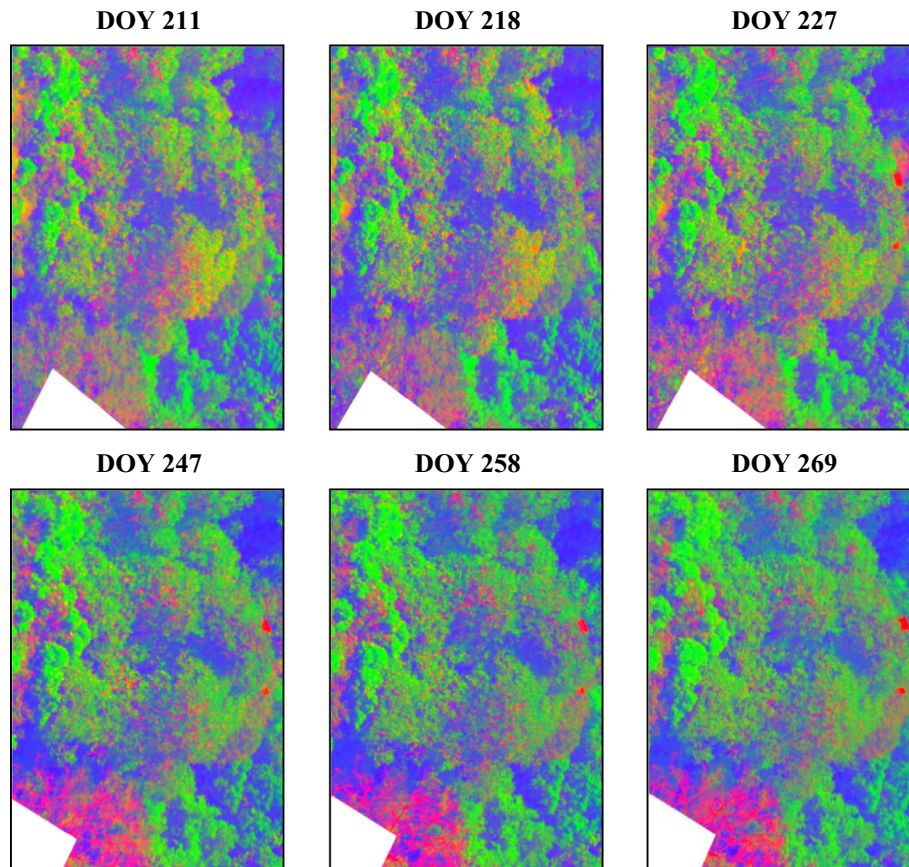


Fig. 4. Color composites of SMA fraction images showing dry season variations over time (July 29–September 25) in green vegetation (green), non-photosynthetic vegetation (red) and shade (blue) for six of the 17 hyperspectral images. The tree species discussed in the text are delineated in Fig. 2. (For interpretation of the references to color in this figure legend, the reader is referred to the web version of this article.)

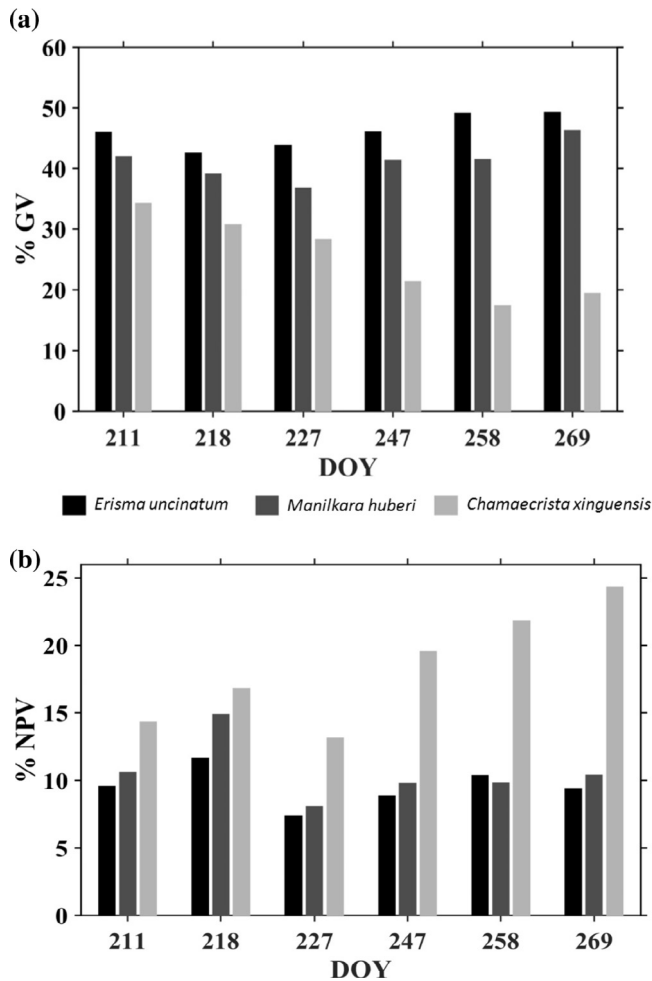


Fig. 5. Bar graph illustration of dry season changes in spectral mixture fractions of (a) green vegetation (GV) and (b) non-photosynthetic vegetation (NPV) for the three species and six of the 17 dates under analysis.

interpretation of the component matrix loadings, PC1 separated the highly reflective *Erisma uncinatum* at the right side of the axis from the other lower reflectance species at the left side. Therefore, brightness increased from the left to the right side of PC1. On the other hand, PC2 separated the deciduous *Chamaecrista xinguensis* with greater amounts of NPV from the evergreen species. In the PC space of Fig. 9, increases in brightness and NPV were generally stronger toward the end of the dry season for *Erisma uncinatum* (gain in leaves) and *Chamaecrista xinguensis* (losses in leaves), respectively. *Manilkara huberi* presented an intermediate phenological pattern between *Erisma uncinatum* and *Chamaecrista xinguensis*.

3.3. Variations in reflectance, vegetation indices and absorption band attributes

In agreement with the PCA results (Figs. 8 and 9), *Erisma uncinatum* had higher mean reflectance than *Manilkara huberi* and *Chamaecrista xinguensis* in green and NIR bands with the largest loadings on PC1 (Fig. 10a and c). On the other hand, great amounts of NPV for *Chamaecrista xinguensis* produced comparatively higher red reflectance (Fig. 10b) and lower NIR reflectance (Fig. 10c) in bands that had large positive and negative PC2 loadings, respectively (Fig. 8). Therefore, the reflectance patterns observed in

Fig. 10 were consistent with the spatial distribution of the PCA scores in Fig. 9.

Reflectance differences over time were also observed for each species and were statistically significant between the beginning and end of the time series at 95% confidence level (t -tests). For *Chamaecrista xinguensis*, differences over time were stronger in the red bands due to increasing deciduousness. For *Erisma uncinatum*, SMA results and the green and NIR reflectance differences observed between the beginning and end of the dry season (Fig. 10) indicated the presence of coupled effects of leaf flushing and reduction in shadows due to changes in SZA and SAA, or in RAA (Figs. 6 and 7). As illustrated in Fig. 11, the role played by leaf flushing detected over the images is to increase the reflectance, especially in the green and NIR spectral regions. Differences between young and old leaves for reflectance spectra extracted from neighboring branches under the same illumination conditions were concentrated in the green region due to lower chlorophyll content of young leaves, and in the NIR region due to differences in leaf structure.

Variations in the described patterns of canopy phenology were also detected after VI determination (Fig. 12). There were statistical differences (95% confidence level) between the species and across the dates, especially for EVI and GRND, for *Erisma uncinatum* and *Chamaecrista xinguensis*, and between August (DOY 210–220) and September (DOY 268). Leaf flushing over *Erisma uncinatum* toward the end of time series produced increases in EVI (Fig. 12a) and GRND (Fig. 12c) because of the observed changes in the NIR and green reflectance in response to the modification in the dominant leaf class in the crown from mature to young leaves (Fig. 11). As demonstrated in previous studies, EVI is strongly dependent on the NIR reflectance at both MODIS (Galvão et al., 2011; Moura et al., 2012) and single leaf scales (Yang et al., 2014). For *Chamaecrista xinguensis*, the NDVI decreased over time due to the reduction in chlorophyll content and the resultant increase in the red reflectance with deciduousness (Fig. 12b).

From the continuum removal analysis, deeper chlorophyll absorption bands centred at 681 nm were observed for *Erisma uncinatum* when compared to the other two species (Fig. 13). A similar pattern was observed for the width and area of this spectral feature, which did not present a well-defined trend for the asymmetry. However, except for *Chamaecrista xinguensis*, the differences were not statistically significant for each species between the period analyzed.

In general, increased chlorophyll contents broaden the 681-nm absorption feature that becomes deeper for a given species, shifting the red-edge position to longer wavelengths in the 690–750 nm range. Our first-order derivative analysis, however, showed variations in the red-edge position between the species and across dates close to the bandwidth of the hyperspectral camera (5 nm). Such differences (results not shown) were not statistically different at 95% confidence level, as indicated by t -tests of means differences between the beginning and end of the observation period.

3.4. MODIS observations at the Tapajós k67 site

In the previous hyperspectral analysis with the tower-based camera, we detected three distinct patterns of canopy phenology: two patterns associated with evergreen species that predominated at the k67 site (*Erisma uncinatum* and *Manilkara huberi*) and one pattern related to a less common deciduous species (*Chamaecrista xinguensis*). For scaling up our tower-based results to a larger footprint, we plotted biweekly long-term mean (2000–2014) of MODIS EVI and GRND corrected for BRDF effects using MAIAC (Fig. 14). According to our results, these two VIs were more sensitive to leaf

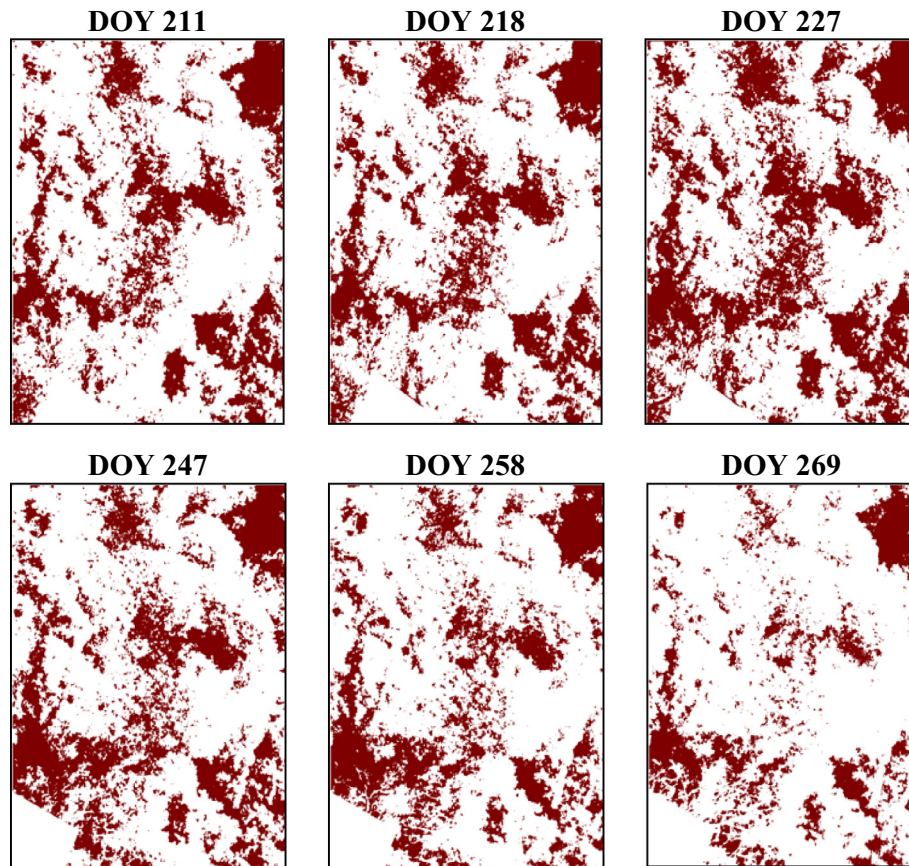


Fig. 6. Spatial and temporal variability in shade fraction for pixels with endmember abundance greater than 60%. The decrease in shade over time is clearly apparent due to decreasing solar zenith angle (SZA), increasing solar azimuth angle (SAA), or decreasing relative azimuth angle (RAA), toward the end of the dry season (DOY 211–269).

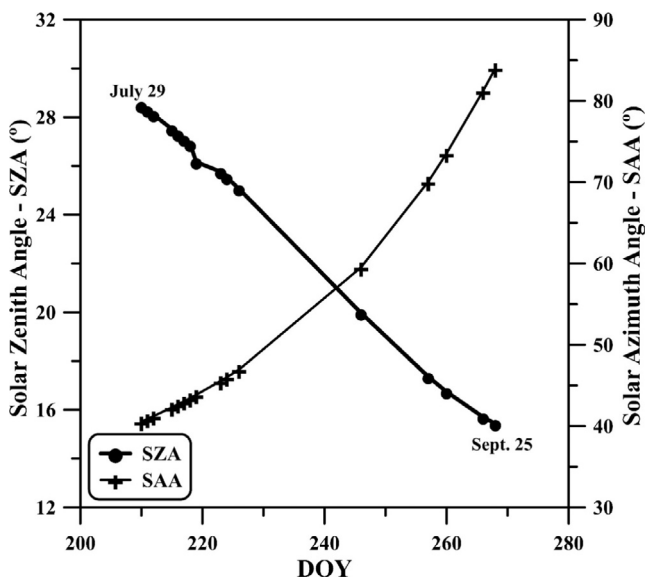


Fig. 7. Temporal changes in solar zenith angle (SZA) and solar azimuth angle (SAA) observed at the time of image collection (11:30 a.m. local time) for each of the 17 dates of hyperspectral image acquisition. The marked change in SZA and relative azimuth angle (RAA; not shown) between July and September contributed to shade variability in the scene, as illustrated in Fig. 6.

flushing than the NDVI because of the respective changes in green and NIR reflectance observed from old to young leaves (Fig. 11).

The VI comparison at a 3 × 3-km MODIS footprint with the modeled phenological observations (leaf demography-ontogeny

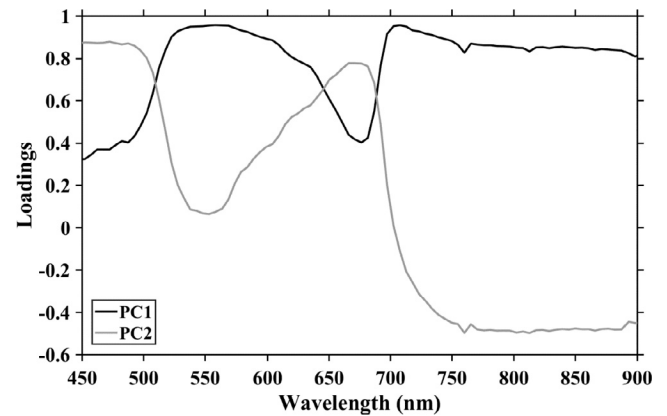


Fig. 8. Component matrix loadings for the first two principal components (PC1 and PC2). PC1 was driven mostly by brightness variations, whereas PC2 was dominated by relative changes in green and non-photosynthetic vegetation (NPV) due to leaf losses.

model) by Wu et al. (2016a) showed that the GRND was closely related to new leaf production at the Tapajós k67 site (Fig. 14). On the other hand, the EVI was more associated with changes in the LAI of mature leaves (3–5 months). Therefore, these observed increases in EVI during the dry season can be related to a proportional increase in mature leaves in relation to young leaves. GRND increased from July to August and then decreased toward September. In contrast, EVI increased over time toward the end of the dry season (Fig. 14). Young bright green leaves (high GRND) constitute

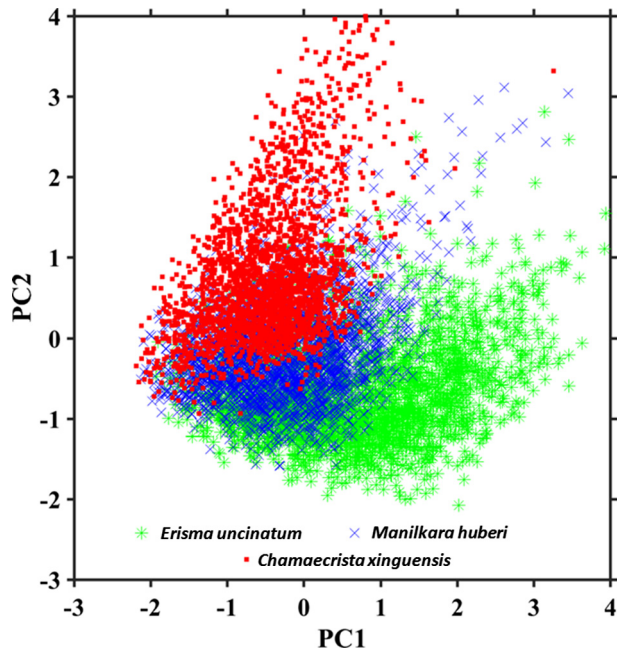


Fig. 9. First two scores from PCA applied to the reflectance of 89 bands (437–898 nm) of the hyperspectral camera, showing canopy spectral variations between three species ($n = 7650$ pixels from 17 dates). In the observation period (July 29–September 25), brightness increased from the left to the right side of PC1 with gains in leaves. NPV increased from the bottom to the top of PC2 with losses in leaves.

a brief phenological stage. These leaves change to mature dark green leaves (lower GRND, but high EVI), a longer-lasting phenological stage. The abundance of this class increases over the dry season as more trees have flushed in the prior dry months.

4. Discussion

Canopy phenology is a vital indicator of environmental controls on species and ecosystems (Cleland et al., 2007; Richardson et al., 2012). A better understanding of vegetation phenology is therefore urgently needed for a better comprehension of climate sensitivity of tropical vegetation (Hilker et al., 2014). The results presented in this study, which is the first hyperspectral investigation using a tower-mounted camera to observe canopy phenology in the Amazon, contribute to this ongoing discussion in two major ways.

First, we have demonstrated, using a detailed study of individual tree crowns observed by the hyperspectral camera at the Tapajós site, a diversity of phenological responses during the 2012 dry season. Our results have shown different stages of phenology for three individual species (*Erisma uncinatum*, *Manilkara huberi* and *Chamaecrista xinguensis*). Different timings and intensity in leaf flushing and leaf shedding affected the GV and NPV fractions obtained from SMA (Figs. 5 and 6); the spatial distribution of PCA scores associated with brightness and deciduousness (Fig. 9); the red, green and NIR reflectance and related VIs (Figs. 10 and 12); and the 681-nm chlorophyll absorption band parameters (Fig. 13). The standard deviation of these spectral attributes was larger after DOY 245 with the closest alignment between the tower camera and the sun as well as with the largest phenological variability observed with the precipitation decrease and the temperature increase (Fig. 1). As discussed by Lopes et al. (2016), flushing in the Amazon is concentrated in the months of low rainfall and occurs in a strategy to exploit the season of high insolation.

The temporal variation in these spectral attributes was therefore affected to some extent by view-illumination effects produced by decreasing SZA, increasing SAA, or modifications in the RAA

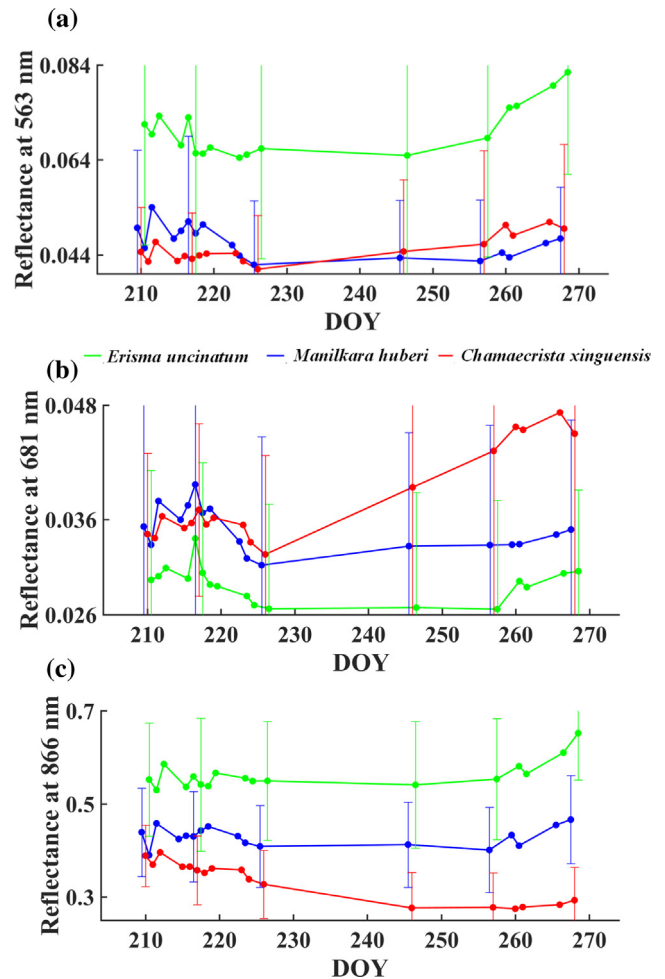


Fig. 10. Dry season variations in mean reflectance of the (a) green, (b) red and (c) near infrared bands of the tower-mounted hyperspectral camera for the 3 species and 17 dates under analysis. The error bars represent the spatial variability of the samples within the tree crowns (mostly driven by differences in shade fraction). Temporal differences between dates of minimum and maximum reflectance were statistically significant for all species at 95% confidence level. (For interpretation of the references to color in this figure legend, the reader is referred to the web version of this article.)

between the camera and the sun, which decreased toward the end of the dry season (Fig. 7). In the SMA, such effects were expressed by decreasing shade fractions over time (Fig. 6). However, they did not explain, for instance, the temporal differences between the two evergreen species with *Erisma uncinatum* presenting clearly leaf flush events in the images that varied in intensity between the trees.

The results presented in our paper confirm previous findings of other two recent tower-based phenological studies in the Amazon basin using multispectral data or RGB cameras (Lopes et al., 2016; Wu et al., 2016a). Importantly, this study demonstrates the usefulness of tower-based cameras to have a comprehensive understanding of the processes that are occurring through time in the canopy and how they influence the vegetation spectral behavior at high spectral resolution. Knowing how the spectra change with physical modifications in the canopy will enhance our knowledge on how these changes affect the spectra from large-scale orbital optical data.

From the three studied species, *Erisma uncinatum* and *Manilkara huberi* alone account for 16% of basal area of the vegetative community of the area and are therefore very important. While arguably measurements of a few tree crowns, or flux tower

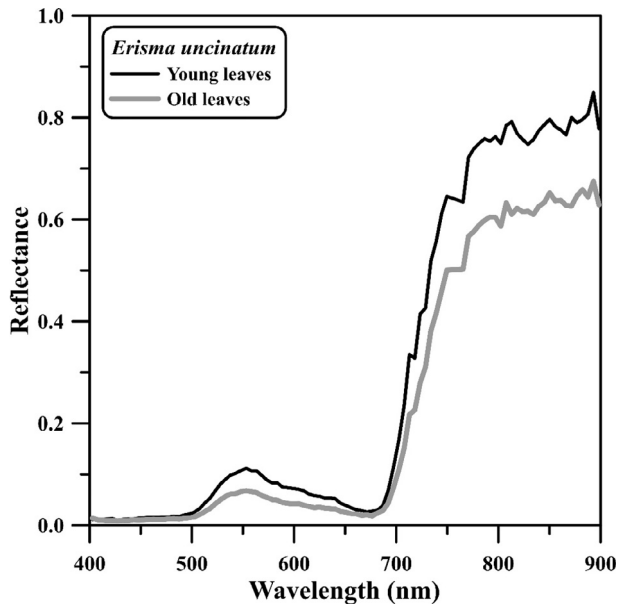


Fig. 11. Spectral reflectance differences between young and old leaves of *Erisma uncinatum* selected from neighboring branches under the same illumination conditions, illustrating changes in the green and near infrared intervals due to leaf flushing.

footprints, are not representative of the entire Amazon basin, the implications of these results are still important, as they track the phenological processes that can be clearly linked with the variation of the spectral signal, demonstrating the heterogeneity of tropical forests. Consequently, the degree of dry season “greening” or “browning” (Huete et al., 2006; Myneni et al., 2007; Restrepo-Coupe et al., 2013) observed by the remote sensing instrumentation will be dependent upon pixel size, viewing geometry, and the relative contribution of species with specific seasonal behavior, in addition to climatological factors.

Often ignored in large-scale ecosystem studies, which sometimes list evergreen tropical forests as a single biome, the marked complexity of the tropical forest biome therefore poses significant challenges for scaling phenological observations from landscape to wide basin levels (Townsend et al., 2008). Observed seasonal trends from coarser scale remote sensing studies (Huete et al., 2006; Myneni et al., 2007) need to be interpreted as seasonal variations in the likelihood of leaf flushing (so called “synchronized” leaf flushing) rather than a homogeneous increase in leaf area across the entire pixel. The exact causes triggering different behavior in different species and individuals of the same species remain poorly understood, as does its representation in earth system models (Restrepo-Coupe et al., 2013). Recent work has suggested that seasonal responses of tropical forest productivity may be a result of the interactions between plant physiology, biotic and abiotic factors (Wu et al., 2016b), as well as biological evolution (Girardin et al., 2016). Integrated studies of environmental and ecological factors constituting eco-physiological conditions on one side, and networking of phenological cameras (Richardson et al., 2012) combined with high resolution remote sensing on the other, are therefore needed to help us better understand these patterns.

As a second contribution, our study has shown that careful consideration of the relationship between phenological responses and spectral reflectance is needed, as physiological changes in plant canopies affect visible and NIR reflectance in very specific ways. For instance, different dynamics in red and NIR reflectance caused different behaviors of NDVI and EVI, arguably the two most fre-

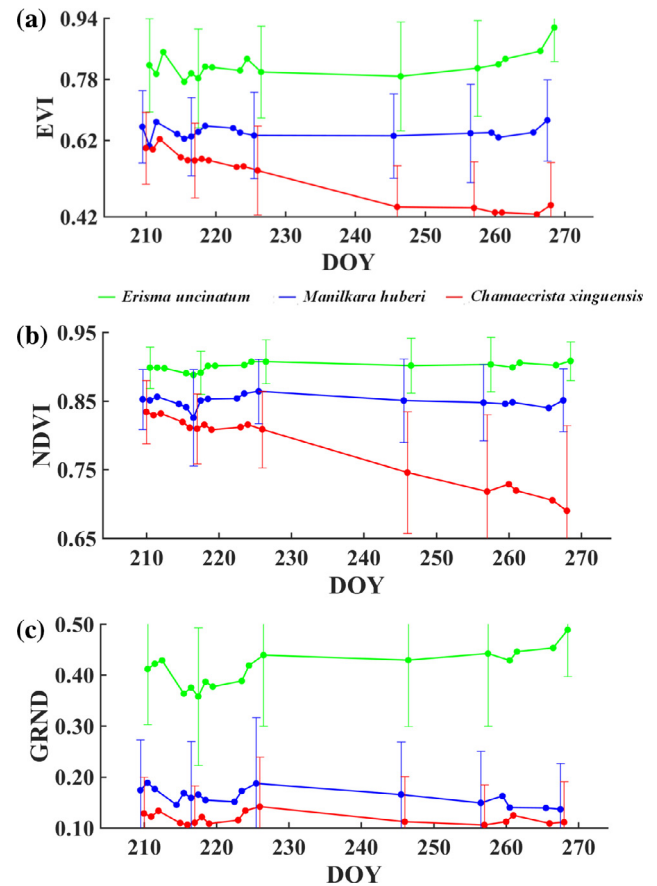


Fig. 12. Dry season variations in (a) Enhanced Vegetation Index (EVI), (b) Normalized Difference Vegetation Index (NDVI) and (c) Green-Red Normalized Difference (GRND) calculated from narrow bands of the hyperspectral camera for the three species and 17 dates under analysis. The error bars represent the spatial variability of the samples within the tree crowns. Temporal differences between dates of minimum and maximum VIs were statistically significant for all species at 95% confidence level. (For interpretation of the references to color in this figure legend, the reader is referred to the web version of this article.)

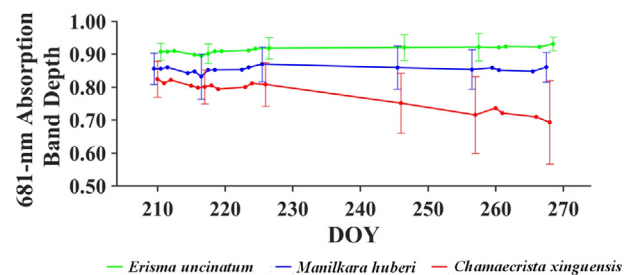


Fig. 13. Temporal variations in the depth of the 681-nm chlorophyll absorption band for the three species from the continuum removal method applied to the hyperspectral images obtained in 17 dates. The error bars represent the spatial variability of reflectance within the tree crowns. Decrease in absorption band depth was associated with leaf loss.

quently used VIs for estimating changes in Amazon seasonality. Briefly, the two VIs reacted differently to the same timeline of phenological changes. Similar findings have been reported in the literature and are a result of different VI formulations (Hilker et al., 2014; Maeda et al., 2016). For example, EVI is largely driven by changes in NIR reflectance, whereas NDVI is the normalized difference between equally weighted NIR and red reflectance (Galvão et al., 2011; Moura et al., 2012).

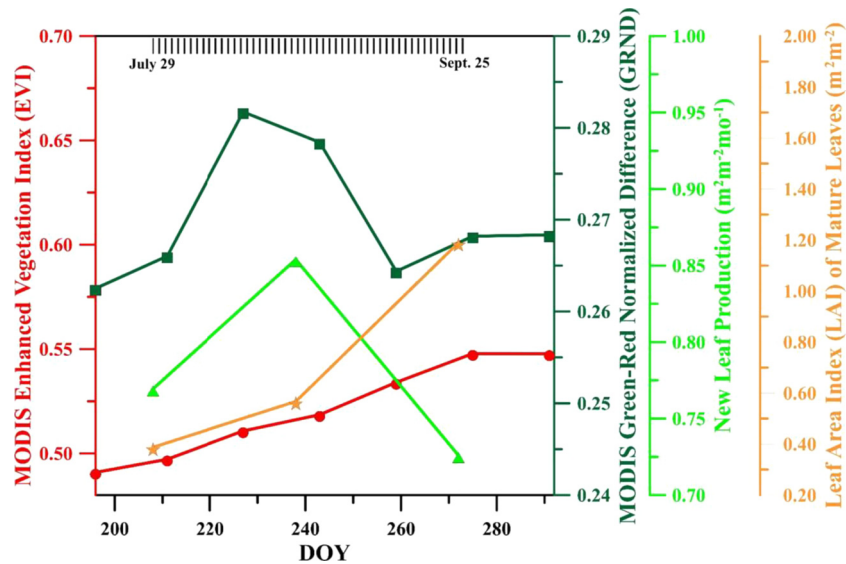


Fig. 14. Temporal changes in long-term means (2000–2014) of MODIS (MAIAC) EVI (red axis) and GRND (dark green axis) compared to the new leaf production (light green axis, leaves 1–2 mo old) and leaf area index of mature leaves (orange axis, 3–5 mo old) modeled by Wu et al. (2016a). Modeled new leaf production at the Tapajós k67 site followed GRND closely, whereas EVI was more related to changes in mature leaf area. (For interpretation of the references to color in this figure legend, the reader is referred to the web version of this article.)

Biophysical interpretations of large scale “greening” and “browning” effects as a result of changes in these VIs need to be made carefully as the underlying physiological behavior may be complex, especially given the spatial heterogeneity demonstrated here on just a few individual trees. For instance, changes in NIR reflectance can be caused by variations in LAI, but can also be just the result of modifications in canopy structure or leaf angle distribution (de Moura et al., 2015). Similarly, increased absorption of visible reflectance is indicative of increased photosynthetic capacity of vegetation, but photosynthesis itself depends on additional factors such as light use efficiency (Demmig-Adams et al., 2008).

In our study, changes in EVI most closely tracked changes in mature leaf area modeled at the landscape level by Wu et al. (2016a) at the Tapajós site, but EVI was not a good indicator of leaf flushing behavior. For instance, a monotonic increase in MODIS observed EVI from July to September, after the BRDF correction by MAIAC, was more consistent with an increase in LAI of mature leaves, because new leaf flushing peaked in August and then declined in September (Fig. 14). Leaf flushing may have little effect on total leaf area (Wu et al., 2016a,b), as abscised leaves are quickly replaced by new grown leaves (Lopes et al., 2016). Nonetheless, young, mature and old leaves have very different capacities to photosynthesize (Kitajima et al., 1997). Consequently, leaf demography is an important driver of photosynthetic potential. These variations may be missed when only observing reflectance sensitive to changes in LAI.

Our findings showed that new leaf flushing was closely observed by the GRND rather than by the EVI. This seems plausible, as absorption of visible radiation is largely driven by leaf pigment concentrations, which, in turn, is closely linked to leaf age (Blackburn, 2007; Doughty and Goulden, 2008; Kitajima et al., 1997; Roberts et al., 1998). For instance, leaf chlorophyll concentrations peak in mature leaves and decline toward senescence.

The relatively large standard deviations in comparison to the variation in seasonal signals presented in the spectral profiles (Figs. 10, 12 and 13) are resultant of the spatial variability within the illuminated part of the tree crowns. While there may still be some effects of canopy shading driving this variation due to imperfect estimates of shadow fractions, these variations show opposite behavior for different species and can therefore not be attributed

solely to sun-sensor effects. Our results are in agreement with previous studies (Hilker et al., 2014; Saleska et al., 2016), but do not support findings on constant canopy structure and greening during the dry season in the Amazon (Morton et al., 2014). Despite the spatial variability within the tree canopies, temporal changes were still statistically significant at 95% confidence level for most of the spectral attributes. Furthermore, even after BRDF correction of MODIS data by the MAIAC, the behavior of the EVI and GRND was not constant over time.

Our results have shown that accurate monitoring of tropical forest phenology is possible from tower and spaceborne remote sensing when considering the spatial heterogeneity of Amazonian forests and the biophysical underpinnings of spectral reflectance behavior in different regions of the electromagnetic spectrum. The current analysis is important to support future studies in the Amazon using planned orbital hyperspectral missions such as the EnMAP and HypSIIRI. All techniques used here can be applied to images of these sensors to link information from future networks of tower-mounted hyperspectral cameras with hyperspectral satellite observations at 30 m spatial resolution.

5. Conclusions

We provided a comprehensive analysis about the spectral components of canopy phenology of three species and compared the data acquired by a tower-mounted hyperspectral camera in the eastern Amazon with BRDF-corrected MODIS (MAIAC) data and modeled LAI/leaf flushing. Our findings showed dry season changes in canopy structure and greenness of the species. In addition, because of the NIR dependence, the EVI was more sensitive to canopy structure than the GRND, which was closely associated with leaf flushing.

The variation in timing and intensity of leaf flushing and leaf shedding for *Erisma uncinatum*, *Manilkara huberi* and *Chamaecrista xinguensis* was mostly expressed by distinct GV and NPV fractions from SMA, different clusters of species in the PCA space, and by modifications in parameters of the 681-nm chlorophyll absorption band from the continuum removal approach. Well-defined trends were not observed for the red-edge spectral position that varied

close to the 5-nm bandwidth of the camera. The most important spectral intervals associated with leaf flushing were the green and NIR regions. Leaf loss in *Chamaecrista xinguensis* increased the red reflectance (reduction in chlorophyll content) and decreased the NIR reflectance due to great amounts of NPV observed for this species in September. The hyperspectral camera data were affected by view-illumination effects, which reduced the amounts of shadows viewed by the sensor cast by neighbor or emergent trees.

View-illumination effects on MODIS data were corrected by the MAIAC. At the k67 tower site, the EVI corrected for BRDF effects monotonically increased from July to September and closely tracked the changes in LAI of mature leaves (3–5 months) modeled by the leaf demography-ontogeny model. The GRND was a better indicator of leaf flushing than the EVI, because the modeled production of new leaves peaked in August and then declined in September. Therefore, the modeled new leaf production at the Tapajós site followed the GRND closely, whereas the EVI was more related to changes in mature leaf area.

Acknowledgements

This work was supported by the GOAmazon project, funded jointly by the U.S. Department of Energy (DOE) (DE-SC0008383), Fundação de Amparo à Pesquisa do Estado de São Paulo (FAPESP) (2013/50533-5 and 2015/23868-1), and Fundação de Amparo à Pesquisa do Estado do Amazonas (FAPEAM) (062.00570/2014). TH was supported by the Conselho Nacional de Desenvolvimento Científico e Tecnológico (CNPq) (PVE 401025/2014-4). The authors thank the reviewers for their comments and suggestions.

References

- Anderson, L.O., Aragão, L.E.O.C., Shimabukuro, Y.E., Almeida, S., Huete, A., 2011. Fraction images for monitoring intra-annual phenology of different vegetation physiognomies in Amazonia. *Int. J. Remote Sens.* 32 (2), 387–408.
- Aragão, L.E.O.C., Malhi, Y., Barbier, N., Lima, A., Shimabukuro, Y., Anderson, L., Saatchi, S., 2008. Interactions between rainfall, deforestation and fires during recent years in the Brazilian Amazonia. *Philos. Trans. R. Soc. Lond. B Biol. Sci.* 363 (1498), 1779–1785. <http://dx.doi.org/10.1098/rstb.2007.0026>.
- Arora, V.K., Boer, G.J., 2005. A parameterization of leaf phenology for the terrestrial ecosystem component of climate models. *Glob. Change Biol.* 11 (1), 39–59. <http://dx.doi.org/10.1111/j.1365-2486.2004.00890.x>.
- Bi, J., Knyazikhin, Y., Choi, S., Park, T., Barichivich, J., Ciais, P., et al., 2015. Sunlight mediated seasonality in canopy structure and photosynthetic activity of Amazonian rainforests. *Environ. Res. Lett.* 10 (6), 064014. <http://dx.doi.org/10.1088/1748-9326/10/6/064014>.
- Blackburn, G.A., 2007. Hyperspectral remote sensing of plant pigments. *J. Exp. Bot.* 58 (4), 855–867. <http://dx.doi.org/10.1093/jxb/erl123>.
- Bonan, G.B., Levis, S., Sitch, S., Vertenstein, M., Oleson, K.W., 2003. A dynamic global vegetation model for use with climate models: concepts and description of simulated vegetation dynamics. *Glob. Change Biol.* 9 (11), 1543–1566. <http://dx.doi.org/10.1046/j.1365-2486.2003.00681.x>.
- Borchert, R., Calle, Z., Strahler, A.H., Baertschi, A., Magill, R.E., Broadhead, J.S., Kamau, J., Njoroge, J., Muthuri, C., 2015. Insolation and photoperiodic control of tree development near the equator. *New Phytol.* 205, 7–13.
- Cerny, C.A., Kaiser, H.F., 1977. A study of a measure of sampling adequacy for factor-analytic correlation matrices. *Multivar. Behav. Res.* 12, 43–47.
- Cho, M.A., Skidmore, A.K., 2006. A new technique for extracting the red edge position from hyperspectral data: The linear extrapolation method. *Remote Sens. Environ.* 101 (2), 181–193. <http://dx.doi.org/10.1016/j.rse.2005.12.011>.
- Clark, R.N., Roush, T.L., 1984. Reflectance spectroscopy: quantitative analysis techniques for remote sensing applications. *J. Geophys. Res.: Solid Earth* 89 (B7), 6329–6340. <http://dx.doi.org/10.1029/JB089iB07p06329>.
- Cleland, E.E., Chuine, I., Menzel, A., Mooney, H.A., Schwartz, M.D., 2007. Shifting plant phenology in response to global change. *Trends Ecol. Evol.* 22 (7), 357–365. <http://dx.doi.org/10.1016/j.tree.2007.04.003>.
- Clevers, J.G.P.W., Gitelson, A.A., 2013. Remote estimation of crop and grass chlorophyll and nitrogen content using red-edge bands on Sentinel-2 and -3. *Int. J. Appl. Earth Observations Geoinf.* 23, 344–351. <http://dx.doi.org/10.1016/j.jag.2012.10.008>.
- Cox, P.M., Betts, R.A., Collins, M., Harris, P.P., Huntingford, C., Jones, C.D., 2004. Amazonian forest dieback under climate-carbon cycle projections for the 21st century. *Theoret. Appl. Climatol.* 78 (1–3), 137–156. <http://dx.doi.org/10.1007/s00704-004-0049-4>.
- D'Odorico, P., Gonsamo, A., Gough, C.M., Bohrer, G., Morison, J., Wilkinson, M., et al., 2015. The match and mismatch between photosynthesis and land surface phenology of deciduous forests. *Agric. For. Meteorol.* 214, 25–38. <http://dx.doi.org/10.1016/j.agrformet.2015.07.005>.
- Demmig-Adams, B., Adams III, W.W., Barker, D.H., Logan, B.A., Bowling, D.R., Verhoeven, A.S., 2008. Using chlorophyll fluorescence to assess the fraction of absorbed light allocated to thermal dissipation of excess excitation. *Physiol. Plant.* 98 (2), 253–264. <http://dx.doi.org/10.1034/j.1399-3054.1996.980206.x>.
- Doughty, C.E., Goulden, M.L., 2008. Seasonal patterns of tropical forest leaf area index and CO₂ exchange. *J. Geophys. Res.* 113, G00B06. <http://dx.doi.org/10.1029/2007JG000590>.
- Frank, D., Reichstein, M., Bahn, M., Thonicke, K., Frank, D., Mahecha, M.D., et al., 2015. Effects of climate extremes on the terrestrial carbon cycle: concepts, processes and potential future impacts. *Glob. Change Biol.* 21 (8), 2861–2880. <http://dx.doi.org/10.1111/gcb.12916>.
- Friedlingstein, P., Cox, P., Betts, R., Bopp, L., von Bloh, W., Brovkin, V., et al., 2006. Climate-carbon cycle feedback analysis: results from the C4 MIP model intercomparison. *J. Clim.* 19 (14), 3337–3353. <http://dx.doi.org/10.1175/JCLI3800.1>.
- Galvão, L.S., dos Santos, J.R., Roberts, D.A., Breunig, F., Marcelo, B., Toomey, M., de Moura, Y.M., 2011. On intra-annual EVI variability in the dry season of tropical forest: a case study with MODIS and hyperspectral data. *Remote Sens. Environ.* 115 (9), 2350–2359. <http://dx.doi.org/10.1016/j.rse.2011.04.035>.
- Gamon, J.A., Rahman, A.F., Dungan, J.L., Schildhauer, M., Huemmrich, K.F., 2006. Spectral network (SpecNet)—what is it and why do we need it? *Remote Sens. Environ.* 103 (3), 227–235. <http://dx.doi.org/10.1016/j.rse.2006.04.003>.
- Garbulsky, M.F., Peñuelas, J., Papale, D., Filella, I., 2008. Remote estimation of carbon dioxide uptake by a Mediterranean forest. *Glob. Change Biol.* 14 (12), 2860–2867. <http://dx.doi.org/10.1111/j.1365-2486.2008.01684.x>.
- Garrity, S.R., Vierling, L.A., Bickford, K., 2010. A simple filtered photodiode instrument for continuous measurement of narrowband NDVI and PRI over vegetated canopies. *Agric. For. Meteorol.* 150.
- Girardin, C.A.J., Malhi, Y., Doughty, C.E., Metcalfe, D.B., Meir, P., de Aguiar-Pasquel, J., et al., 2016. Seasonal trends of Amazonian rainforest phenology, net primary productivity, and carbon allocation. *Global Biogeochem. Cycles* 30 (5), 700–715. <http://dx.doi.org/10.1002/2015GB005270>.
- Green, A.A., Berman, M., Switzer, P., Craig, M.D., 1988. A transformation for ordering multispectral data in terms of image quality with implications for noise removal. *IEEE Trans. Geosci. Remote Sens.* 26 (1), 65–74. <http://dx.doi.org/10.1109/36.3001>.
- Guan, K., Pan, M., Li, H., Wolf, A., Wu, J., Medvigy, D., Caylor, K.K., Sheffield, J., Wood, E.F., Malhi, Y., Liang, M., 2015. Photosynthetic seasonality of global tropical forests constrained by hydroclimate. *Nat. Geosci.* 8 (4), 284–289.
- Guanter, L., Kaufmann, H., Segl, K., Foerster, S., Rogass, C., Chabrilat, S., et al., 2015. The EnMAP spaceborne imaging spectroscopy mission for earth observation. *Remote Sensing* 7 (7), 8830–8857. <http://dx.doi.org/10.3390/rs70708830>.
- Hilker, T., Leeuwen, M., Coops, N.C., Wulder, M.A., Newnham, G.J., Jupp, D.L.B., Culvenor, D.S., 2010. Comparing canopy metrics derived from terrestrial and airborne laser scanning in a Douglas-fir dominated forest stand. *Trees* 24 (5), 819–832. <http://dx.doi.org/10.1007/s00468-010-0452-7>.
- Hilker, T., Lyapustin, A.I., Tucker, C.J., Hall, F.G., Myneni, R.B., Wang, Y., et al., 2014. Vegetation dynamics and rainfall sensitivity of the Amazon. *Proc. Natl. Acad. Sci.* 111 (45), 16041–16046. <http://dx.doi.org/10.1073/pnas.1404870111>.
- Hochberg, E.J., Roberts, D.A., Dennison, P.E., Hulley, G.C., 2015. Special issue on the hyperspectral infrared imager (HyspIRI): emerging science in terrestrial and aquatic ecology, radiation balance and hazards. *Remote Sens. Environ.* 167, 1–5.
- Huete, A., Didan, K., Miura, T., Rodriguez, E.P., Gao, X., Ferreira, L.G., 2002. Overview of the radiometric and biophysical performance of the MODIS vegetation indices. *Remote Sens. Environ.* 83 (1–2), 195–213.
- Huete, A.R., Didan, K., Shimabukuro, Y.E., Ratana, P., Saleska, S.R., Hutyrá, L.R., et al., 2006. Amazon rainforests green-up with sunlight in dry season. *Geophys. Res. Lett.* 33 (6), L06405. <http://dx.doi.org/10.1029/2005GL025583>.
- Kitajima, K., Mulkey, S., Wright, S., 1997. Decline of photosynthetic capacity with leaf age in relation to leaf longevities for five tropical canopy tree species. *Am. J. Bot.* 84 (5), 702.
- Kokaly, R.F., Skidmore, A.K., 2015. Plant phenolics and absorption features in vegetation reflectance spectra near 1.66 μm. *Int. J. Appl. Earth Obs. Geoinf.* 43, 55–83. <http://dx.doi.org/10.1016/j.jag.2015.01.010>.
- Lee, J.E., Frankenberg, C., van der Tol, C., Berry, J.A., Guanter, L., Boyce, C.K., Fisher, J. B., Morrow, E., Worden, J.R., Asefi, S., Badgley, G., 2013. Forest productivity and water stress in Amazonia: Observations from GOSAT chlorophyll fluorescence. *Proc. R. Soc. Lond. B: Biol. Sci.* 280 (1761), 20130171.
- Lopes, A.P., Nelson, B.W., Wu, J., de Graça, P.M.L., et al., 2016. Leaf flush drives dry season green-up of the Central Amazon. *Remote Sens. Environ.* 182. <http://dx.doi.org/10.1016/j.rse.2016.05.009>.
- Lyapustin, A.I., Martonchik, J., Wang, Y., Laszlo, I., Korkin, S., 2011. Multiangle implementation of atmospheric correction (MAIAC): 1. Radiative transfer basis and look-up tables. *J. Geophys. Res.: Atmos.* 116(D3).
- Maeda, E.E., Moura, Y.M., Wagner, F., Hilker, T., Lyapustin, A.I., Wang, Y., et al., 2016. Consistency of vegetation index seasonality across the Amazon rainforest. *Int. J. Appl. Earth Obs. Geoinf.* 52, 42–53. <http://dx.doi.org/10.1016/j.jag.2016.05.005>.
- Malhi, Y., Roberts, J.T., Betts, R.A., Killeen, T.J., Li, W., Nobre, C.A., 2008. Climate Change, Deforestation, and the Fate of the Amazon. <http://dx.doi.org/10.1126/science.1146961> (January 11).
- Moreira, R.C., Galvão, L.S., 2010. Variation in spectral shape of urban materials. *Remote Sensing Lett.* 1 (3), 149–158. <http://dx.doi.org/10.1080/01431161003692032>.

- Morton, D.C., Nagol, J., Carabajal, C.C., Rosette, J., Palace, M., Cook, B.D., et al., 2014. Amazon forests maintain consistent canopy structure and greenness during the dry season. *Nature* 506 (7487), 221–224. <http://dx.doi.org/10.1038/nature13006>.
- de Moura, Y.M., Hilker, T., Lyapustin, A.I., Galvão, L.S., dos Santos, J.R., Anderson, L.O., et al., 2015. Seasonality and drought effects of Amazonian forests observed from multi-angle satellite data. *Remote Sens. Environ.* 171, 278–290. <http://dx.doi.org/10.1016/j.rse.2015.10.015>.
- Moura, Y.M., Galvao, L.S., dos Santos, J.R., Roberts, D.A., Breunig, F.M., 2012. Use of MISR/Terra data to study intra- and inter-annual EVI variations in the dry season of tropical forest. *Remote Sens. Environ.* 127, 260–270. <http://dx.doi.org/10.1016/j.rse.2012.09.013>.
- Myneni, R.B., Yang, W., Nemani, R.R., Huete, A.R., Dickinson, R.E., Knyazikhin, Y., et al., 2007. Large seasonal swings in leaf area of Amazon rainforests. *Proc. Natl. Acad. Sci. USA* 104 (12), 4820–4823. <http://dx.doi.org/10.1073/pnas.0611338104>.
- Phillips, O.L., Aragão, L.E.O.C., Lewis, S.L., Fisher, J.B., Lloyd, J., López-gonzález, G., et al., 2009. Drought sensitivity of the amazon rainforest. *Science* 323 (5919), 1344–1347.
- Restrepo-Coupe, N., da Rocha, H.R., Hutyrá, L.R., da Araujo, A.C., Borma, L.S., Christoffersen, B., et al., 2013. What drives the seasonality of photosynthesis across the Amazon basin? A cross-site analysis of eddy flux tower measurements from the Brasil flux network. *Agric. For. Meteorol.* 182–183, 128–144. <http://dx.doi.org/10.1016/j.agrformet.2013.04.031>.
- Richardson, A.D., Anderson, R.S., Arain, M.A., Barr, A.G., Bohrer, G., Chen, G., et al., 2012. Terrestrial biosphere models need better representation of vegetation phenology: results from the North American Carbon Program Site Synthesis. *Glob. Change Biol.* 18 (2), 566–584. <http://dx.doi.org/10.1111/j.1365-2486.2011.02562.x>.
- Richardson, A.D., Jenkins, J.P., Braswell, B.H., Hollinger, D.Y., Ollinger, S.V., Smith, M.-L., 2007. Use of digital webcam images to track spring green-up in a deciduous broadleaf forest. *Oecologia* 152 (2), 323–334. <http://dx.doi.org/10.1007/s00442-006-0657-z>.
- Roberts, D.A., Nelson, B.W., Adams, J.B., Palmer, F., 1998. Spectral changes with leaf aging in Amazon caatinga. *Trees* 12, 315–325.
- Roberts, D.A., Smith, M.O., Adams, J.B., 1993. Green vegetation, nonphotosynthetic vegetation, and soils in AVIRIS data. *Remote Sens. Environ.* 44, 255–269.
- Saleska, S.R., Didan, K., Huete, A.R., da Rocha, H.R., 2007. Amazon forests green-up during 2005 drought. *Science (New York, NY)* 318 (5850), 612. <http://dx.doi.org/10.1126/science.1146663>.
- Saleska, S.R., Wu, J., Guan, K., Araújo, A., Huete, A.R., Restrepo-Coupe, N., 2016. Dry-season greening of Amazon forests evidence from ecological studies. *Nature* 531. <http://dx.doi.org/10.1038/nature13006>.
- Samanta, A., Ganguly, S., Hashimoto, H., Devadiga, S., Vermote, E., Knyazikhin, Y., et al., 2010. Amazon forests did not green-up during the 2005 drought. *Geophys. Res. Lett.* 37 (5). <http://dx.doi.org/10.1029/2009GL042154>.
- Tortini, R., Hilker, T., Coops, N., Nesic, Z., 2015. Technological advancement in tower-based canopy reflectance monitoring: the AMSPEC-III system. *Sensors* 15 (12), 32020–32030. <http://dx.doi.org/10.3390/s151229906>.
- Townsend, A.R., Asner, G.P., Cleveland, C.C., 2008. The biogeochemical heterogeneity of tropical forests. *Trends Ecol. Evol.* 23 (8), 424–431. <http://dx.doi.org/10.1016/j.tree.2008.04.009>.
- van der Meer, F., 2004. Analysis of spectral absorption features in hyperspectral imagery. *Int. J. Appl. Earth Obs. Geoinf.* 5 (1), 55–68. <http://dx.doi.org/10.1016/j.jag.2003.09.001>.
- Woebbecke, D.M., Meyer, G.E., Von Bargen, K., Mortensen, D.A., 1995. Color indices for weed identification under various soil, residue, and lighting conditions. *Trans. ASAE* 38, 259–269.
- Wu, J., Albert, L.P., Lopes, A.P., Restrepo-Coupe, N., Hayek, M., Wiedemann, K.T., et al., 2016a. Leaf development and demography explain photosynthetic seasonality in Amazon evergreen forests. *Science* 351 (6276). <http://dx.doi.org/10.1126/science.aad5068>.
- Wu, J., Guan, K., Hayek, M., Restrepo-Coupe, N., Wiedemann, K.T., Xu, X., Wehr, R., Christoffersen, B.O., Miao, G., Silva, R., Araujo, A.C., 2016b. Partitioning controls on Amazon forest photosynthesis between environmental and biotic factors at hourly to interannual timescales. *Glob. Change Biol.* <http://dx.doi.org/10.1111/gcb.13509>.
- Xu, L., Samanta, A., Costa, M.H., Ganguly, S., Nemani, R. R., Myneni, R.B., 2011. Widespread decline in greenness of Amazonian vegetation due to the 2010 drought. *Geophys. Res. Lett.* 38(7), n/a–n/a. <http://dx.doi.org/10.1029/2011GL046824>.
- Yang, X., Tang, J., Mustard, J.F., 2014. Beyond leaf color: comparing camera-based phenological metrics with leaf biochemical, biophysical, and spectral properties throughout the growing season of a temperate deciduous forest. *J. Geophys. Res.: Biogeosci.* 119, 181–191.
- Zelazowski, P., Sayer, A.M., Thomas, G.E., Grainger, R.G., 2011. Reconciling satellite-derived atmospheric properties with fine-resolution land imagery: insights for atmospheric correction. *J. Geophys. Res.* 116 (D18), D18308. <http://dx.doi.org/10.1029/2010JD015488>.